Journal of Radiological Protection

Official journal of the Society for Radiological Protection

PAPER

Evaluation of mean conversion coefficients from air-kerma to $H^*(10)$ using secondary and transmitted x-ray spectra in the diagnostic radiology energy range

To cite this article: A H Lopez Gonzales *et al* 2016 *J. Radiol. Prot.* **36** 842

IOP Publishing | Society for Radiological Protection Journal of Radiological Protection
J. Radiol. Prot. **36** (2016) 842–857 doi:10.1088/0952-4746/36/4/842

Evaluation of mean conversion coefficients from air-kerma to $H^*(10)$ using secondary and transmitted x-ray spectra in the diagnostic radiology energy range

A H Lopez Gonzales[1], J C Santos[1], L Mariano[1], A Tomal[2] and P R Costa[1]

[1] Instituto de Física da Universidade de São Paulo, São Paulo, Brazil
[2] Instituto de Física Gleb Wataghin, Universidade Estadual de Campinas, São Paulo, Brazil

E-mail: ahlopezg@usp.br

Received 13 May 2016, revised 4 August 2016
Accepted for publication 12 September 2016
Published 14 October 2016

Abstract

Ambient dose equivalent $H^*(10)$ is an operational quantity recommended by the IAEA to establish dose constraints in area monitoring for external radiation. The direct measurement of $H^*(10)$ is not common due to the complexity in the calibration procedures of radiation monitors involving the use of expanded and aligned radiation fields. Therefore, conversion coefficients are used to assess $H^*(10)$ from the physical quantity air-kerma. Conversion coefficients published by international commissions, ICRU and ICRP, present a correlation with the radiation beam quality. However, Brazilian regulation establishes 1.14 Sv Gy^{-1} as unique conversion coefficient to convert air-kerma into $H^*(10)$, disregarding its beam quality dependence. The present study computed mean conversion coefficients from secondary and transmitted x-ray beams in order to improve the current assessment of $H^*(10)$. The weighting of conversion coefficients corresponding to monoenergetic beams with the spectrum energy distribution in terms of air-kerma was used to compute the mean conversion coefficients. In order to represent dedicated chest radiographic facilities, an anthropomorphic phantom was used as scatter object of the primary beam. Secondary x-ray spectra were measured in the diagnostic energy range at scattering angles of 30°, 60°, 90° 120° and 150° degrees. Barite mortar plates were used as attenuator of the secondary beam to produce the corresponding transmitted x-ray spectra. Results show that the mean conversion coefficients are about 43% higher than the recommended value accepted by Brazilian regulation. For secondary radiation measured at 100 kV the mean coefficient should be 1.46 Sv Gy^{-1}, which represent the higher value in the mean

coefficient set corresponding to secondary beams. Moreover, for transmitted x-ray beams at 100 kV, the recommended mean conversion coefficient is 1.65 Sv Gy^{-1} for all barite mortar plate thickness and all scattering angles. An example of application shows the discrepancy in the evaluation of secondary shielding barriers in a controlled area when the shielding goals is evaluated. The conclusion based on these results is that a unique coefficient may not be adequate for deriving the $H^*(10)$.

Keywords: ambient dose equivalent, air-kerma, secondary and transmitted x-ray spectra, mean conversion coefficient

(Some figures may appear in colour only in the online journal)

1. Introduction

The International Commission on Radiation Units and Measurements, ICRU, and the International Commission on Radiological Protection, ICRP, are entities responsible to develop and promulgate internationally accepted recommendations on radiation related to quantities and units, measurement procedures and reference data used on radiation protection of individuals and populations. These recommendations have been adopted by different countries in their local regulations. Two of the first actions taken jointly by ICRU and ICRP were the definition of quantities and units to be used in radiological protection and the establishment of dose limits for radiation workers (ICRU 1993, 2011, ICRP 2007, Jennings 2007). For instance, the radiological protection quantity effective dose is used to establish dose limits and dose constraints (ICRP, 1991, 2007). However, the effective dose is not directly measureable and therefore, it is necessary the use of the corresponding operational quantity to its estimation (ICRU 1998). For external radiation and area monitoring, the ambient dose equivalent at 10 mm depth of the ICRU sphere, $H^*(10)$, is used to derive the effective dose (IAEA 2007, 2014). The derivation process is through the use of adequate conversion coefficients between $H^*(10)$ and effective dose (ICRU 1998).

Brazilian regulation (Brazil 1998) adopts $H^*(10)$ as reference quantity to verify conformity with dose constraints in area monitoring. The calibration of radiation monitors to represent its reading in $H^*(10)$ requires the use of expanded and aligned radiation fields (Stadtmann 2001, ICRU 2011) resulting in calibration procedures with high complexity of implementation. Therefore, the dosimetric quantity air-kerma is used in order to facilitate the assessment of $H^*(10)$ through conversion coefficients and then compare with the dose constraints established in the regulation. Conversion coefficients relating air-kerma to $H^*(10)$ for monoenergetic beams are published in table A21 of the ICRU report 57 (ICRU 1998) and they present a strong beam energy dependence. On the other hand, spectrometric studies show variations on the energy distribution of x-ray beams produced in imaging installations depending of the x-ray beam type considered (Santos and Costa 2014, Santos *et al* 2016). Therefore, a specific conversion coefficient from air-kerma to $H^*(10)$ for each x-ray beam produced from different practices or when the x-ray beams pass through different attenuators is necessary (Peixoto *et al* 1992). Brazilian regulation establishes 1.14 Sv Gy^{-1} as unique conversion coefficient to convert air-kerma into $H^*(10)$ disregarding its beam energy dependence. The value established by the Brazilian regulation is used in radiometric survey and to compute shielding barriers. Therefore, to assess more realistic conversion coefficients, the ICRU report 57 recommends the use of mean conversion coefficients obtained by weighting the conversion coefficients computed from monoenergetic beams with the broad energy spectra (ICRU 1998, Stadtmann 2001) produced in radiological facilities. Kharrati and Zarrad (2004) developed

a computational method to predict mean conversion coefficients by weighting the conversion coefficients published in table A21 of the ICRU report 57 with unfiltered primary x-ray spectra based on the computational models of Boone and Siebert (1997). The coefficients published by ICRU report 57 are based on previous works (Wagner *et al* 1985, Grosswendt *et al* 1988) and are related to monoenergetic photons with energies from 10 keV to 10 MeV. As originally presented, this methodology was applied to determine mean conversion coefficients for narrow primary x-ray spectra. Previous work used that methodology to compute mean conversion coefficients for broad primary radiation beams (Santos *et al* 2016).

The present work aims to improve the assessment of $H^*(10)$ adapting the Kharrati and Zarrad method to compute mean conversion coefficients considering the modification on the energy distribution of the x-ray spectra scattered by an anthropomorphic phantom and transmitted by barite mortar plates. Previous works computed the mean conversion coefficient to evaluate primary barriers in diagnostic radiological facilities using x-ray beams transmitted through anthropomorphic phantom, grid anti-scatter and barite mortar plates (Santos and Costa 2014, Santos *et al* 2016). The barite mortar of barium sulfite was chosen because is largely applied in Brazil to build shielding barriers in radiological facilities (Benvindo da Luz and Magalhães 2005). The term transmitted x-ray spectra refers to the experimental spectra measured behind the barrier positioned at different scatter angles with respect to the central axis of the primary beam. It includes non-attenuated scattered photons and photons scattered by the barite mortar plate. Moreover, it is presented a typical situation of radiometric survey where it was determined the $H^*(10)$ using the conversion coefficient, 1.14 Sv Gy^{-1}, and the corresponding coefficient obtained in the present study.

2. Methods and materials

2.1. Calculation of the mean conversion coefficients

In this study, the Kharrati and Zarrad (2004) methodology was extended to secondary beams with scattering angles of 30°, 60°, 90°, 120° and 150° degrees and for secondary beams transmitted through of barite mortar plates with thickness defined in table 1. Kharrati and Zarrad used the x-ray spectra computed by Boone and Siebert (1997) to determine the corresponding mean conversion coefficients. However, in this work, it was used experimental x-ray spectra from broad beam with inherent filtration of 2.2 mmBe and additional filtration of 3.04 mmAl. Boone and Seibert performed a polynomial interpolation to compute the tungsten x-ray spectra from measured constant potential x-ray spectra published by Fewell *et al* (1981).

The mean conversion coefficient, $\overline{C}_k$, relates the air-kerma, K_{air}, with the ambient dose equivalent, $H^*(10)$, as shown in equation (1).

$$H^*(10) = \overline{C}_k K_{air} \tag{1}$$

In this work, equation (2) represents the adaptation of the Kharrati and Zarrad methodology (Kharrati and Zarrad 2004, Santos *et al* 2016) for secondary and transmitted x-ray beams.

$$\overline{C}_k = \frac{\int_0^{E_{max}} C_k(E)\Phi(E,\theta)E\left(\frac{\mu_{en}(E)}{\rho}\right)_{air}\exp(-\mu(E)x)\mathrm{d}E}{\int_0^{E_{max}} \Phi(E,\theta)E\left(\frac{\mu_{en}(E)}{\rho}\right)_{air}\exp(-\mu(E)x)\mathrm{d}E} \tag{2}$$

Table 1. Thickness specification for the barite mortar plates.

Identification	Thickness (mm)
B10	10.6 (5)
B15	16.4 (6)
B20	21.2 (7)
B25	24.8 (4)

Note: The numbers in brackets represent uncertainties in the last decimal place.

Where $C_k(E)$ are the monoenergetic conversion coefficients from table A21 of the ICRU report 57, $\Phi(E,\theta)$ is the photon fluence spectrum defined as the photon fluence of energy E at scatter angle θ per energy interval, for a primary x-ray spectra the angle $\theta = 0$. The angle between the primary central ray and the scatter direction defines the scatter angle θ as shown in figure 1. $\mu_{en}(E)/\rho$ is the mass-energy absorption coefficient, being equivalent to the mass-energy transfer coefficient for diagnostic energies. The term $\exp(-\mu(E)x)$ is the attenuation factor as a function of the barite mortar plate thickness, x, with linear attenuation coefficient $\mu(E)$. Moreover, the air-kerma for secondary or transmitted radiation, $K_{air}(E,x,\theta)$, is defined in equation (3).

$$K_{air}(E,x,\theta) = \Phi(E,\theta)E\left(\frac{\mu_{en}(E)}{\rho}\right)_{air}\exp(-\mu(E)x) \tag{3}$$

Therefore, equation (4) is used the compute the mean conversion coefficient from the x-ray spectrum expressed in terms of air-kerma.

$$\overline{C}_k = \frac{\int_0^{E_{max}} C_k(E)K_{air}(E,x,\theta)\mathrm{d}E}{\int_0^{E_{max}} K_{air}(E,x,\theta)\mathrm{d}E} \tag{4}$$

In the same way, equation (5) was used to determine the mean energy, $\overline{E}_m$, for each spectrum.

$$\overline{E}_m = \frac{\int_0^{E_{max}} EK_{air}(E,x,\theta)\mathrm{d}E}{\int_0^{E_{max}} K_{air}(E,x,\theta)\mathrm{d}E} \tag{5}$$

All mean conversion coefficients were plotted as a function of the first half value layer (HVL) and the mean energy of the corresponding x-ray spectrum. The HVL is related to the beam hardening and is expressed by the thickness, x, of a reference material (usually aluminum). The HVL was computed for each beam using a code developed in MatLab R2011a environment (The MathWorks Inc., USA) from the air-kerma x-ray spectrum (Tomal *et al* 2014).

2.2. Measurement of the x-ray spectra

The development of experimental setups to measure both secondary and transmitted x-ray spectra were carried out in order to compute the corresponding mean conversion coefficients

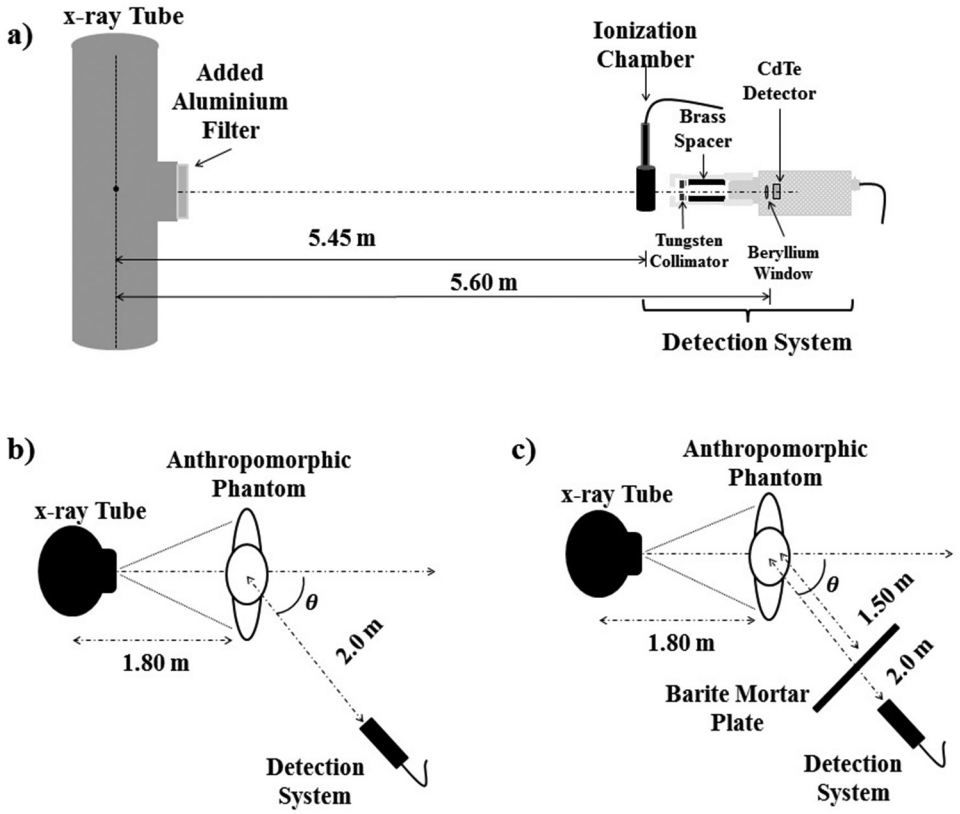

Figure 1. Experimental setups used to measure (a) primary x-ray spectra, (b) secondary x-ray spectra and (c) transmitted x-ray spectra through a barite mortar plate. The representations of the setup components for each case are not in the real scale.

using equation (4). Previously to the measurement of secondary and transmitted x-ray spectra, primary x-ray spectra were measured using the experimental arrangement presented in figure 1(a). The Philips MCN 421 x-ray tube was used as x-ray source and the tube voltages chosen were from 40 kV up to 150 kV in steps of 10 kV. All measurements were performed using an additional aluminum filtration of 3.04 mm in the x-ray tube. This filtration is used to obtain the RQR 5 x-ray beam quality with 2.58 mmAl of HVL and 0.71 of homogeneity coefficient, as defined in Technical Report Series No 457 (IEC 2005, IAEA 2007). The detection system for primary beams consisted in a PTW 30 cm^3 ionization chamber model TW23361 (PTW, Inc., Freiburg, Germany) coupled with an electrometer model Unidos E, both calibrated in an PTB (PTB, Braunschweig, Germany) accredited traceable secondary standard laboratory, and the PX4 digital pulse processor with a $3 \times 3 \times 1$ mm^3 CdTe detector model XR-100T-CdTe (Amptek, Inc., Bedford, MA, USA) were considered as the spectrometry system. The CdTe semiconductor detector has been widely used in x-ray and gamma-ray spectrometry (DiCastro *et al* 1984, Redus *et al* 2009, Tomal *et al* 2015). A distance of 5.60 m was considered between CdTe detector and x-ray source in order to avoid damage in the detector or spectral distortion due to pile-up effect and dead time losses. A tungsten collimator with 2 mm of diameter was placed at front of the Beryllium window as showed in

figure 1(a). The CdTe detector has been shielded with a lead copper and brass box, in order to avoid contribution of undesirable scatter radiation from the walls of room. The ionization chamber was positioned in front of the CdTe detector in order to assess the air-kerma at 5.45 m from the focal spot. The air-kerma rate at 5.45 m was about 5.4 uGy mAs^{-1} at 150 kV of tube voltage and corrections of temperature and pressure were taken in consideration for all air-kerma measurements. The air-kerma that reaches the spectrometer was considered as the ion chamber read corrected by the inverse-square law and ion chamber calibration coefficient. The primary beam emitted by the Philips MCN 421 x-ray tube has been validated in previous works (Lopez Gonzales *et al* 2015, Santos *et al* 2016).

Figure 1(b) presents the experimental apparatus used to measure the secondary x-ray spectra at 30°, 60°, 90°, 120° and 150° degrees with respect to the central axis of the primary beam. The primary beam impinges on the surface thoracic region of an anthropomorphic phantom (RANDO® Man, Alderson Research Laboratories) located at 1.80 m from the focal spot. According to White (1978) the elemental composition of Alderson muscle is C 66.81%, O 21.13%, H 8.87%, N 3.10% and Sb 0.08% and for Alderson lung is C 73.94%, O 18.14%, H 5.74%, N 2.01% and Sb 0.16%. The field size at the thoracic region of the scatter object was $29 \times 27\,cm^2$. The arrangement in figure 1(b) was intended to reproduce dedicated chest radiographic facilities. For secondary and transmitted beams, an $1800\,cm^3$ ionization chamber model Radcal 10×5-1800 (Radcal, Corp., California, USA), calibrated in terms of air-kerma and manufactured for radiation protection purposes was used to permit measurements at low exposure levels. The distance between the center of scatter region and detection system was 2 m. The secondary radiation is the sum of the scatter radiation plus leakage radiation. Figure 1(c) shows the experimental arrangement to measure transmitted x-ray spectra through barite mortar plate with thickness specified in table 1. The measurement time for each spectrum was about 3 h using a CdTe detector. The air-kerma measurement was performed in air-kerma rate mode and relatively short exposure time. Therefore, the ionization chamber was not affected by any significant drift. The barite mortar is a shielding material widely used in Brazil to shield diagnostic imaging facilities (Benvindo da Luz and Magalhães 2005). The barite mortar is manufactured by the GRX group (GRX group, Sao Paulo, Brazil). The plates used in this work have a useful area of $70 \times 70\,cm^2$, they were used in a previous work (Santos *et al* 2016) to calculate mean conversion coefficients between air-kerma and $H^*(10)$ considering primary shielding barriers. The plates were used as attenuator of the secondary radiation and its chemical compositions is described by Santos (2013).

All x-ray spectra were normalized to the measured air-kerma and by the tube current-time product, mAs, and corrected to 1 m distance from the focal spot to obtain mGy/mAs@1 m units. For secondary and transmitted spectra, the relation between the air-kerma with the phantom central-point distance does not follow exactly the inverse square law (Fehrenbacher *et al* 1996). However, the inverse-square law is applied only for comparison between the spectra and it does not affect the computation of the corresponding mean conversion coefficient. A monitor PTW ionization chamber model 34014, (PTW, Inc., Freiburg, Germany), was used to track the x-ray tube output. The readings of the ionization chamber model Radcal 10×5-1800 (Radcal, Corp., California, USA) presented an uncertainty of 10.1% for a 95% confidence interval. The energy calibration of the spectrometry system was carried out using three calibration sources, Am-241, Ba-133 and Eu-152 which have photon energy emission in the diagnostic energy range. MCA was set to 1024 channels with gain of $30.31\times$ and the rise time discrimination (RTF) function turned off. The calibration factor was 0.1710(3) keV per channel, representing the angular coefficient in a linear fitting. The raw spectra were corrected using the stripping procedure (DiCastro *et al* 1984) considering the

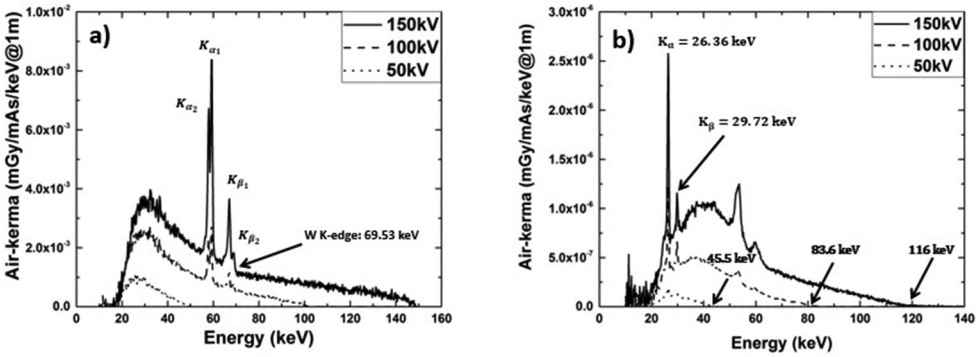

Figure 2. (a) Primary spectra at 50, 100 and 150 kV. The characteristic peaks corresponding to 57.9, 59.3, 67.2 and 69 keV is presented as well as the influence of the auto-absorption of the tungsten K-edge at 69, 53 keV over 150 kV x-ray spectrum. (b) Secondary spectra at 50, 100 and 150 kV and 90° degrees of scatter angle. The ^{51}Sb K_α and K_β characteristic x-ray is showed as well as the higher-energy photon for each spectrum predicted by the Compton scattering model.

detector efficiency, escape of Cd and Te K x-rays photons and escape of Compton-scattered photons. The major distortion in the raw spectra is due to the escape peaks of Cd and Te, since in the diagnostic energy range the photoelectric effect prevails in the detector material. The correction software implemented in MatLab R2011a environment (The MathWorks Inc., USA) was developed in the Physics Institute of Sao Paulo University, based on the work of Tomal *et al* (2015). This work was assembled and performed at the Laboratory of Radiation Dosimetry and Medical Physics, Physics Institute of Sao Paulo University.

3. Results and discussions

3.1. X-ray spectra

3.1.1. Primary and secondary x-ray spectra. A set of primary spectra from 40 to 150 kV at intervals of 10 kV was measured. Figure 2(a) illustrates three primary x-ray spectra corresponding to voltages of 50, 100 and 150 kV. In this figure, we noted that the inherent filtration and the added filtration remove all photons with energy lower than 20 keV. Figure 2(a) also shows four peaks, identified as $K_{\alpha 1}$, $K_{\alpha 2}$, $K_{\beta 1}$ and $K_{\beta 2}$, on the spectra corresponding to 100 and 150 kV, which represent the fluorescent x-ray emission of the tungsten target. The edge presented in the 150 kV x-ray spectrum is caused by the self-absorption inside the tungsten target corresponding to energy of tungsten K-edge at 69.53 keV.

Five secondary spectra corresponding to scatter angles of 30°, 60°, 90°, 120° and 150° were measured for each primary spectrum. Figure 2(b) illustrates the air-kerma distribution of secondary spectra measured at 50, 100 and 150 kV and with 90° degrees of scatter angle. Figure 2(b) shows the fluorescent radiation produced onto the anthropomorphic phantom corresponding to ^{51}Sb K_α and K_β characteristic x-ray at 26.36 and 29.72 keV. Despite the ^{51}Sb represents 0.16% of the total mass of the Alderson phantom lung (White 1978), the presence of the characteristic radiation is recurrent in all secondary spectra. The leakage radiation is lower than the scatter radiation in two orders of magnitude. Therefore, figure 2(b) shows principally the scatter component of the secondary spectrum. The Compton scattering model predicts the energy of a scattered photon by a free electron. In figure 2(b), the end point of each

spectrum corresponds to the scattering of the photon with the highest energy in the primary spectrum by a scattering angle of 90° degrees.

The scatter fraction is defined as the ratio of the scattered air-kerma at 1 m from the center of the primary beam area on the patient to the primary air-kerma at 1 m from the x-ray tube divided by the primary beam area at 1 m from the source (NCRP 2004). Table A1 of the appendix A presents scatter fractions computed for each secondary beam measured in this work.

3.1.2. Transmitted x-ray spectra. Four barite mortar plates with thicknesses shown in table 1 were used to produce the transmitted x-ray spectra. For each plate thickness the transmitted spectra at five different angles, 30°, 60°, 90°, 120° and 150° were measured. Figure 3 shows five x-ray spectra transmitted through the barite mortar plate B10 at tube voltage of 150 kV. The leakage radiation reaches the same order of magnitude than the transmitted spectrum especially for higher scattering angles, in contrast of the secondary spectrum case. The contribution of the leakage radiation is reflected over the high energy region on the transmitted spectrum. Figure 3 also shows two peaks at 32.2 and 36.3 keV corresponding to K_α and K_β Barium characteristic radiation. The intensity of the characteristic peak increases with the increment of the scatter angle because for higher scatter angles the scattered photons lose more energy in their interaction into the phantom. Therefore, this phenomenon increases the photoelectric absorption in the barite mortar plate and then the corresponding fluorescent emission.

The mean energy for each x-ray spectrum was computed using the equation (5). Figure 4(a) shows the mean energy corresponding to secondary spectra as a function of the tube voltage. Figure 4(b) shows the mean energy computed from transmitted x-ray spectra passing through the barite mortar plate B20 as a function of the tube voltage.

3.2. Mean conversion coefficients from air-kerma to H(10)*

Equation (4) was used to compute the mean conversion coefficients weighting the coefficients related to monoenergetic beams with the corresponding air-kerma x-ray spectrum. From figures 5–7 are presented the mean conversion coefficients as a function of the mean energy and the HVL corresponding to each spectrum measured in the present study. The uncertainty for each computed coefficient was assessed using the Poisson distribution for each channel of the x-ray spectrum. Figure 5(a) shows the mean conversion coefficients as a function of the mean energy corresponding to secondary beams scattered in angles of 30°, 60°, 90°, 120° and 150° degrees with respect to the axis of the primary beam. Mean conversion coefficients related to primary beam scattered at 120° degrees and transmitted through barite mortar plates as a function of the plate thickness are presented in figure 5(b).

Coefficients related to mean energies above 40 keV are higher than 1.14 Sv Gy^{-1}, value adopted in local regulation. Therefore, for radiometric survey the established coefficient would be underestimating the ambient dose equivalent $H^*(10)$. In this work, the computed coefficients are about 36% higher than 1.14 Sv Gy^{-1} at 150 kV and 30° degrees scatter angle. Figure 5(b) shows the small variation of the coefficients with the plate thickness, e.g. for 120 kV, the higher variation between them is 1.57%.

Figure 6 shows a comparison between the mean conversion coefficients related to primary beams, secondary beams measured at scattering angle of 30° degrees and for transmitted beams through B25 barite mortar plate with thickness presented in table 1. They are also compared with the values obtained from the analytical function of Wagner *et al* (1985) and the value established in local regulation (1.14 Sv Gy^{-1}). Figure 6 also shows the small variation

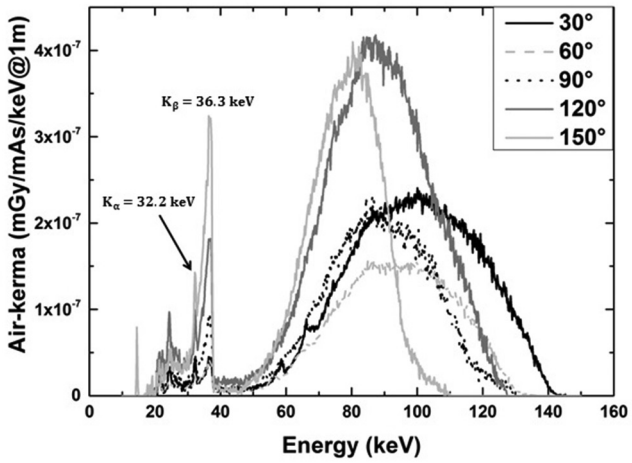

Figure 3. Transmitted x-ray spectra through B10 barite mortar plate at 30°, 60° 90°, 120° and 150° of scatter angle corresponding to 150 kV. The detached characteristic lines are barium K_α and K_β emissions corresponding to 32.2 and 36.3 keV, respectively.

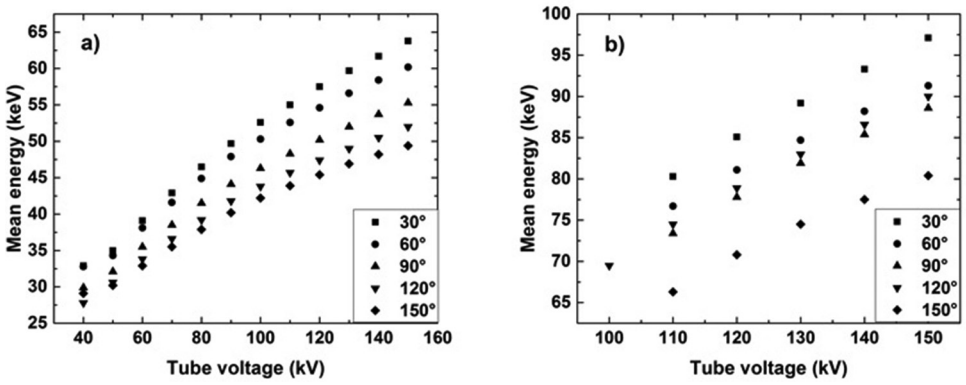

Figure 4. (a) Mean energy corresponding to secondary x-ray spectra and (b) computed from transmitted x-ray spectra passing through the barite mortar plate B20, as a function of the tube voltage and for scattering angles of 30°, 60°, 90°, 120° and 150° degrees.

with the mean energy of the coefficients related to transmitted beams corresponding to primary beam scattered at 30° degrees and transmitted by B25 barite mortar plate, which are named as T_30°_B25. The higher difference between them is 1.54%.

Figures 7(a) and (b) present all mean conversion coefficients computed in this work as a function of the HVL and the mean energy, respectively.

Equation (6) represents the analytical function proposed by Wagner *et al* (1985) to fit the mean conversion coefficients showed in figures 7(a) and (b).

$$\overline{C}_{\mathrm{k}}(E) = \frac{z(E)}{a[z(E)]^2 + bz(E) + c} + d\,x\,\arctan\{gz(E)\} \tag{6}$$

In equation (6), $z(E) = \ln(E/E')$, E is the mean energy (or HVL) in keV (or mmAl), and E', a, b, c, d and g are the fitting parameters of the function obtained by applying regression methods

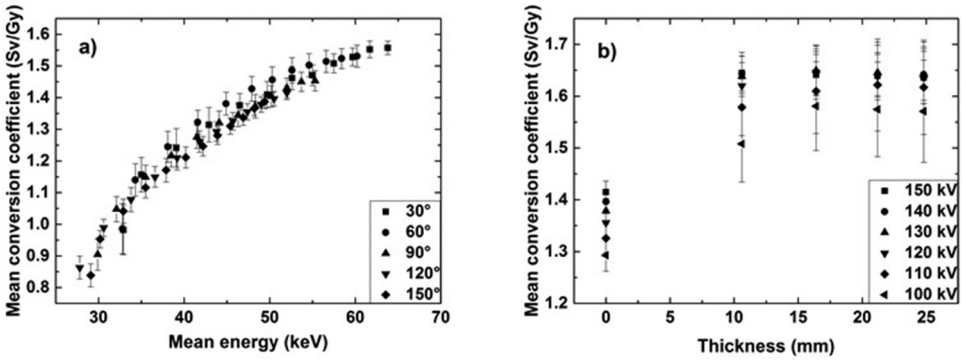

Figure 5. (a) Mean conversion coefficients as a function of the mean energy of each spectrum for secondary beams scattered in angles of 30°, 60°, 90°, 120° and 150° degrees and (b) as a function of the plate thickness corresponding to x-ray beams scattered at 120° degrees.

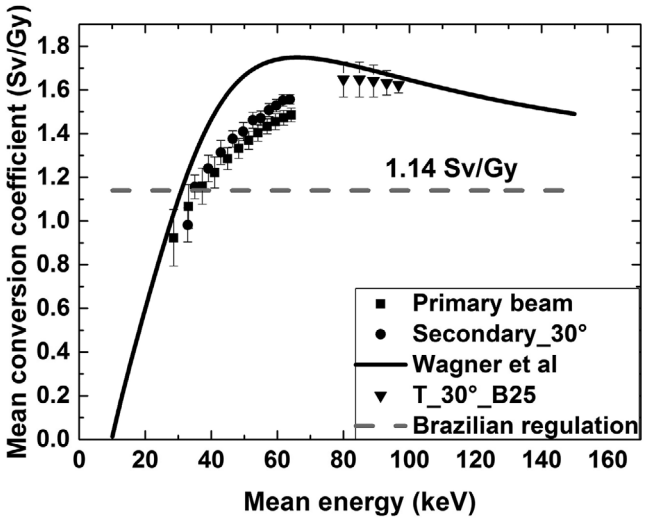

Figure 6. Comparison between mean conversion coefficients related to primary, secondary and transmitted beams through B25 barite mortar plate as a function of mean energy. Is also shown the conversion coefficients related to monoenergetic beams derived by the analytical function of Wagner *et al* (1985) and the constant value adopted by the Brazilian regulation.

and statistical weight experimental input data. Table 2 shows the fitting parameters of equation (6), for the points shown in figures 7(a) and (b).

3.3. Example of application

As a practical use of the mean conversion coefficients for secondary beams transmitted through barite mortar plates is presented a typical radiometric survey in a diagnostic radiology department. Figure 8 shows typical design of a conventional radiology room where a hypothetical radiometric survey was conducted in order to assess the exposure levels within

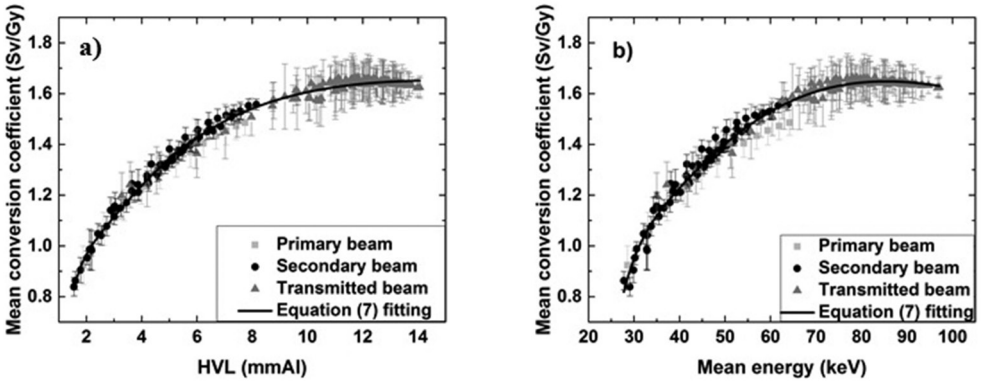

Figure 7. (a) All mean conversion coefficients computed in this work as a function of the half value layer (HVL) and (b) the mean energy. The line represents a fitting with equation (6).

Table 2. Fitting parameters of equation (6) representing the mean conversion coefficient as a function of the half value layer (HVL) and mean energy.

	The fit parameters Refereeing to figure 7(a)	The fit parameters Refereeing to figure 7(b)
Parameters	Value	Value
E'	0.97 (8)	22.1 (9)
a	0.0021 (4)	0.004 (1)
b	0.013 (7)	0.012 (8)
c	0.055 (5)	0.032 (4)
d	−21 (8)	−22 (9)
g	0.6 (1)	1.1 (2)
	$R^2 = 0.99$	$R^2 = 0.98$

Note: The numbers in brackets represent uncertainties in the last decimal place.

the control booth. The secondary beam consists of leakage radiation emitted by the x-ray tube plus the scattered radiation at 120° degrees considering the location of the control booth.

The radiometric survey procedure is done by locating three reference points (a, b, c) inside the control booth, at 3 m from the center of the patient, and measuring exposure levels in terms of air-kerma. Consider that the control booth is shielded with 20 mm of barite mortar. For chest examination, the x-ray tube voltage was set in 120 kV (Dixon and Simpkin 1998). Consider a total workload of 0.22 mA min/patient and 300 patients/week as total explorations (common typical values in chest radiographic facilities) according to NCRP 147 (NCRP 2004). A radiometric survey following the arrangement illustrated in figure 8 provided a hypothetical exposure data, in terms of air-kerma rate, of about 0.068 mGy/week. The corresponding $H^*(10)$ assessed using the conversion coefficient 1.14 Sv Gy^{-1} is 0.076 mGy/week and using 1.64 Sv Gy^{-1} as mean conversion coefficient computed in the present study is 0.11 mGy/week. The $H^*(10)$ assessed using 1.64 Sv Gy^{-1} are about 43% higher than the $H^*(10)$ obtained using the 1.14 Sv Gy^{-1} conversion coefficient. The radiation protection goal for the control booth (dose constraint for occupational exposure) is established in

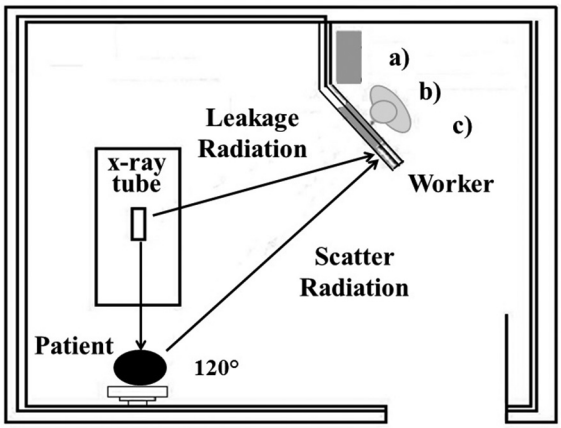

Figure 8. Typical design for a control booth in a radiographic x-ray room, adapted from NCRP 147 (NCRP 2004). The letters inside the control booth indicate three points on which were done a radiometric survey in order to evaluate the radiation exposure. In this situation the primary beam is scattered at 120° degrees.

0.1 mSv/week (ICRP 2007). Therefore, the present example shows that the established value underestimate the $H^*(10)$ and produces contradictory conclusions in terms of shielding adequacy for the area considered.

4. Conclusions

Mean conversion coefficients relating air-kerma to $H^*(10)$ were computed taking into account the energy distribution of secondary and transmitted experimental x-ray spectra following the recommendation of the ICRU report 57 for polyenergetic beams used in dedicated chest radiographic facilities. The air-kerma x-ray spectrum of the secondary beams depends on the scatter angle and the spectrum has contributions of the Sb fluorescence emission presents in the anthropomorphic phantom composition. The air-kerma x-ray spectrum of the transmitted beams depends on the thickness of the barite mortar plate and the spectrum is composed by a continuum photon distribution resulting from transmitted and scattered (by the barium mortar plate) photons plus the Barium x-ray fluorescence emission produced in the plate used. All mean conversion coefficients are shown in figure 7 and in the appendix B, in tables B1–B5, as a function of the mean energy and HVL of the corresponding beam. The results highlight the energy dependence of the conversion coefficients and strengthens the recommendation of ICRU 57.

Additionally, the use of 1.14 Sv Gy^{-1} defined by Brazilian regulation to estimate $H^*(10)$ can carries in an underestimation of this quantity and allow dose levels higher than those established by proper regulation. For instance, the results achieved in the present study are about 43% higher than the value obtained using the coefficient recommended by local regulation. Therefore, $H^*(10)$ obtained by the constant coefficient 1.14 Sv Gy^{-1} may not be adequate for representing environmental doses to evaluate the adequacy of the shielding barrier. As a recommendation, for secondary scatter radiation at 100 kV the mean coefficient should be 1.46 Sv Gy^{-1}, which represent the higher value in the mean coefficients set corresponding to the secondary beams. Moreover, for transmitted x-ray beams at 100 kV, the suggested mean

conversion coefficient is 1.65 Sv Gy^{-1} for all barite mortar plate thickness and all scattering angles.

Finally, the mean conversion coefficients computed in this work could be applied to other shielding materials as a good approximation taking into account the mean energy and HVL of the corresponding x-ray beam.

Acknowledgments

The authors thank the CAPES/PROEX and FAPESP (2011/04721-9) for financial support of the Master Degree Scholarships, the FAPESP for partially funding this work under the project *Estudo experimental das relações entre kerma no ar e equivalente de dose ambiente para o cálculo de barreiras primárias em salas radiológicas* (2010/12237-7), and the CNPq/FAPESP for funding of the project INCT — Metrology of ionizing radiation in medicine (2008/57863-2).

Conflict of interest

The authors declare that they have no conflict of interest.

Appendix A. Scatter fractions

Table A1. Scatter fraction for secondary spectra.

kV\Degree	30°	60°	90°	120°	150°
40	2.31	0.43	0.78	2.23	3.54
50	2.39	0.60	0.91	2.58	4.18
60	2.58	0.76	1.06	2.94	4.66
70	2.80	0.93	1.21	3.24	5.09
80	3.03	1.11	1.36	3.50	5.43
90	3.23	1.27	1.51	3.69	5.63
100	3.44	1.42	1.63	3.91	5.90
110	3.61	1.56	1.74	4.06	6.01
120	3.78	1.68	1.84	4.16	6.16
130	3.90	1.78	1.91	4.25	6.24
140	4.03	1.89	1.99	4.31	6.35
150	4.20	1.97	2.06	4.39	6.39

Note: The x-ray beam size at 1 m of the x-ray tube was 159.1 cm^2. The corresponding units are 10^{-6} cm^{-2} and the uncertainty is 9.6% of the value.

Appendix B. Mean conversion coefficients

All mean conversion coefficients are presented in tables B1–B5 corresponding to primary, secondary and transmitted x-ray spectra measured in this work.

Table B1. Mean conversion coefficients from air-kerma to $H^*(10)$ obtained from primary and secondary x-ray beams.

Voltage (kV)	Primary (Sv Gy^{-1})	30° (Sv Gy^{-1})	60° (Sv Gy^{-1})	90° (Sv Gy^{-1})	120° (Sv Gy^{-1})	150° (Sv Gy^{-1})
40	0.92 (14)	0.98 (7)	0.99 (8)	0.90 (5)	0.86 (3)	0.84 (3)
50	1.07 (9)	1.16 (5)	1.14 (5)	1.05 (4)	0.99 (2)	0.95 (2)
60	1.16 (7)	1.24 (6)	1.24 (4)	1.15 (4)	1.08 (3)	1.04 (4)
70	1.22 (5)	1.31 (5)	1.32 (3)	1.22 (3)	1.15 (3)	1.12 (3)
80	1.29 (3)	1.38 (3)	1.38 (3)	1.28 (3)	1.21 (3)	1.17 (3)
90	1.33 (3)	1.41 (4)	1.43 (3)	1.32 (3)	1.26 (3)	1.21 (3)
100	1.37 (3)	1.46 (3)	1.46 (4)	1.34 (3)	1.29 (3)	1.25 (3)
110	1.40 (2)	1.47 (3)	1.49 (4)	1.37 (3)	1.33 (2)	1.28 (2)
120	1.43 (2)	1.51 (3)	1.50 (4)	1.40 (3)	1.36 (2)	1.31 (2)
130	1.45 (2)	1.53 (2)	1.51 (4)	1.43 (3)	1.38 (2)	1.34 (2)
140	1.47 (2)	1.55 (2)	1.52 (4)	1.45 (3)	1.40 (2)	1.37 (2)
150	1.49 (2)	1.56 (2)	1.53 (4)	1.45 (3)	1.41 (2)	1.39 (2)

Table B2. Mean conversion coefficients from air-kerma to $H^*(10)$ obtained from transmitted x-ray beams through B10 barite mortar plate.

Voltage (kV)	30° (Sv Gy^{-1})	60° (Sv Gy^{-1})	90° (Sv Gy^{-1})	120° (Sv Gy^{-1})	150° (Sv Gy^{-1})
70	—	—	—	—	1.20 (32)
80	—	—	—	1.24 (16)	1.24 (16)
90	1.61 (6)	1.57 (7)	1.45 (10)	1.36 (9)	1.30 (9)
100	1.65 (5)	1.64 (6)	1.55 (9)	1.51 (7)	1.40 (9)
110	1.66 (5)	1.66 (5)	1.61 (8)	1.58 (5)	1.49 (6)
120	1.66 (4)	1.66 (4)	1.64 (7)	1.62 (4)	1.57 (4)
130	1.65 (3)	1.66 (4)	1.65 (8)	1.64 (4)	1.61 (5)
140	1.64 (4)	1.65 (4)	1.65 (7)	1.64 (3)	1.63 (5)
150	1.63 (3)	1.65 (4)	1.65 (6)	1.64 (4)	1.65 (3)

Table B3. Mean conversion coefficients from air-kerma to $H^*(10)$ obtained from transmitted x-ray beams through B15 barite mortar plate.

Voltage (kV)	30° (Sv Gy^{-1})	60° (Sv Gy^{-1})	90° (Sv Gy^{-1})	120° (Sv Gy^{-1})	150° (Sv Gy^{-1})
100	1.65 (8)	—	1.58 (17)	1.58 (8)	—
110	1.66 (7)	1.66 (10)	1.63 (11)	1.61 (8)	1.59 (12)
120	1.66 (7)	1.66 (7)	1.65 (10)	1.65 (5)	1.62 (8)
130	1.65 (4)	1.65 (7)	1.65 (9)	1.65 (5)	1.65 (7)
140	1.63 (4)	1.65 (7)	1.65 (8)	1.65 (4)	1.66 (5)
150	1.62 (3)	1.64 (6)	1.64 (8)	1.64 (4)	1.66 (5)

Table B4. Mean conversion coefficients from air-kerma to $H^*(10)$ obtained from transmitted x-ray beams through B20 barite mortar plate.

Voltage (kV)	30° (Sv Gy^{-1})	60° (Sv Gy^{-1})	90° (Sv Gy^{-1})	120° (Sv Gy^{-1})	150° (Sv Gy^{-1})
100	—	—	—	1.57 (9)	—
110	1.66 (8)	1.66 (8)	1.61 (11)	1.62 (8)	1.58 (12)
120	1.65 (8)	1.66 (8)	1.65 (8)	1.64 (6)	1.64 (9)
130	1.65 (6)	1.65 (8)	1.65 (8)	1.65 (5)	1.65 (7)
140	1.64 (5)	1.65 (8)	1.64 (7)	1.64 (4)	1.65 (7)
150	1.63 (4)	1.64 (7)	1.64 (7)	1.64 (4)	1.65 (6)

Table B5. Mean conversion coefficients from air-kerma to $H^*(10)$ obtained from transmitted x-ray beams through B25 barite mortar plate.

Voltage (kV)	30° (Sv Gy^{-1})	60° (Sv Gy^{-1})	90° (Sv Gy^{-1})	120° (Sv Gy^{-1})	150° (Sv Gy^{-1})
100	—	—	—	1.57 (9)	—
110	1.65 (8)	—	—	1.62 (9)	—
120	1.65 (8)	1.65 (7)	1.63 (9)	1.64 (7)	1.58 (11)
130	1.64 (7)	1.64 (7)	1.64 (8)	1.64 (5)	1.63 (9)
140	1.63 (5)	1.64 (7)	1.64 (7)	1.64 (5)	1.64 (7)
150	1.62 (3)	1.63 (5)	1.64 (7)	1.64 (5)	1.64 (7)

References

ANVISA 1998 Portaria n°453, de 1°de junho de 1998 *Agência Nacional De Vigilância Sanitária Brazil*

Benvindo da Luz A and Magalhães B C A 2005 Barita *Comunicação técnica elaborada para edição do livro Rochas and Minerais Industriais: Uso e especificações*, CETEM-MCT: Centro de tecnologia mineral-Ministério da ciência e tecnologia pp 263–77

Boone J M and Seibert J A 1997 An accurate method for computer-generating tungsten anode x-ray spectra from 30 to 140 kV *Med. Phys.* **24** 1661–70

DiCastro E, Pani R, Pellegrini R and Bacci C 1984 The use of cadmium telluride detectors for the qualitative analysis of diagnostic x-ray spectra *Phys. Med. Biol.* **29** 1117

Dixon R L and Simpkin D J 1998 Primary shielding barriers for diagnostic x-ray facilities: a new model *Health Phys.* **74** 181–9

Fehrenbacher G, Panzer W and Tesfu K 1996 *Spectra of Diagnostic X-Rays Scattered by a Water Phantom* GSF-Forschungszentrum f. Umwelt u. Gesundheit

Fewell T R, Shuping R E, Hawkins K R, United States, Bureau of Radiological Health and Division of Electronic Products 1981 *Handbook of Computed Tomography X-Ray Spectra* (Rockville, MD: US Department of Health and Human Services, Public Health Service, Food and Drug Administration, Bureau of Radiological Health)

Grosswendt B, Hohlfeld K, Kramer H M and Selbach H J 1988 Conversion factors for ICRU dose equivalent quantities for the calibration of radiation protection dosimeters (PTB-Dos–11e) *Germany*

IAEA 2007 *Dosimetry in Diagnostic Radiology: an international Code of Practice* (Vienna: International Atomic Energy Agency)

IAEA 2014 *Radiation Protection and Safety of Radiation Source: International Basic Safety Standards* (*IAEA Safety Standards Series*) (Vienna: International Atomic Energy Agency)

ICRP 1991 *1990 Recommendations of the International Commission on Radiological Protection* (*Annals of the ICRP*, *ICRP Publication 60* vol 21) pp 1–3

ICRP 2007 *The 2007 Recommendations of the International Commission on Radiological Protection* (*Annals of the ICRP, ICRP Publication 103* vol 37) pp 2–4

ICRU 1993 *Quantities and Units in Radiation Protections Dosimetry* (*ICRU Report No. 51*) (Bethesda, MD: ICRU)

ICRU 1998 *Conversion Coefficients for Use in Radiological Protection Against External Radiation* (*ICRU Report No. 57*) (Bethesda, MD: ICRU)

ICRU 2011 *Fundamental Quantities and Units for Ionizing Radiation* (*ICRU Report No. 85a*) (Bethesda, MD: ICRU)

IEC 2005 *Medical Diagnostic X-Ray Equipment—Radiation Conditions for Use in the Determination of Characteristics* (*IEC 61267*) (Geneva: International Electrotechnical Commission)

Jennings W A 2007 Evolution over the past century of quantities and units in radiation dosimetry *J. Radiol. Prot.* **27** 5

Kharrati H and Zarrad B 2004 Computation of conversion coefficients relating air Kerma to Hp(0.07,alpha), Hp(10,alpha), and $H^*(10)$ for x-ray narrow spectrum from 40 to 140 kV *Med. Phys.* **31** 277–84

Lopez Gonzales A H, Tomal A and Costa P R 2015 Evaluation of characteristic-to-total spectrum ratio: comparison between experimental and a semi-empirical model *Appl. Radiat. Isot.* **100** 27–31

NCRP 2004 *Structual Shielding Design for Medical X-Ray Imaging Facilities* (*NCRP Report No. 147*) (Bethesda, MD: NCRP)

Peixoto J E, Drexler G and Zankl M 1992 Attenuation factors for x-rays in terms of ambient and effective dose equivalent *Radiat. Prot. Dosim.* **43** 119–21

Redus R H, Pantazis J A, Pantazis T J, Huber A C and Cross B J 2009 Characterization of CdTe detectors for quantitative x-ray spectroscopy *IEEE Trans. Nucl. Sci.* **56** 2524–32

Santos J C 2013 Estudo experimental das relações entre kerma no ar e equivalente de dose ambiente para o cálculo de barreiras primárias em salas radiológicas. Dissertação de Mestrado, IF-USP: Instituto de Física-Universidade de São Paulo.

Santos J C and Costa P R 2014 Evaluation of the effective energy of primary and transmmitted workload weighted x-ray spectra *Radiat. Phys. Chem.* **95** 221–3

Santos J C, Mariano L, Tomal A and Costa P R 2016 Evaluation of conversion coefficients relating air-kerma to $H^*(10)$ using primary and transmitted x-ray spectra in the diagnostic radiology energy range *J. Radiol. Prot.* **36** 117

Stadtmann H 2001 Dose quantities in radiation protection and dosemeter calibration *Radiat. Prot. Dosim.* **96** 21–6

Tomal A, Cunha D M and Poletti M E 2014 Comparison of beam quality parameters computed from mammographic x-ray spectra measured with different high-resolution semiconductor detectors *Radiat. Phys. Chem.* **95** 217–20

Tomal A, Santos J C, Costa P R, Lopez Gonzales A H and Poletti M E 2015 Monte Carlo simulation of the response functions of CdTe detectors to be applied in x-ray spectroscopy *Appl. Radiat. Isot.* **100** 32–7

Wagner S R, Grosswendt B, Selbach H-J, Siebert B R L, Harvey J R and Mill A J 1985 Unified conversion functions for the new ICRU operational radiation protection quantities *Radiat. Prot. Dosim.* **12** 5

White D R 1978 Tissue substitutes in experimental radiation physics *Med. Phys.* **5** 467–79